

Asymmetrical Six-phase GaN-based Drive Performance Analysis with Variable Switching Frequency Control

Maitane Carrasco¹, Amaia Lopez-de-Heredia¹ and Irma Villar¹

¹ Department of Power Electronics
Ikerlan Basque Research Centre (BRTA)

José María Arizmendiarieta Pasealekua, 2, 20500 Arrasate, Gipuzkoa (Spain)
Phone: +0034 943 712 400

Abstract. This paper analyses the performance of a GaN-based multiphase drive when a variable switching frequency control is implemented for EV applications. The GaN-based inverters allow a wide switching frequency range, and the power losses of the inverter are reduced in comparison with other technologies such as Si. To be able to benefit from this wide switching frequency range, a variable switching frequency control with the objective of maintaining a ratio frequency $m_f = 17$ is implemented. This control reduces the switching frequency losses above 30% in the three analysed speed points in comparison with maintaining a constant switching frequency. Hence, an efficiency improvement is achieved with the variable switching frequency control tackling one of the main problems of the EV.

Key words. Multiphase, WBG, variable switching frequency control, IRFOC.

1. Introduction

Nowadays, the demand in the market for Electric Vehicles (EV) has increased exponentially. Moreover, this demand in the market is expected to increase further due to the policies adopted by the European Parliament towards climate goals such as Fit for 55. However, their efficiency, reliability, cost, and lack of autonomy are still a problem.

To tackle the problem of efficiency and reliability in EV, Silicon (Si) devices of the inverter are replaced by Wide BandGap (WBG) devices. Some of the features of this technology are low on-resistance, high efficiency and they allow a wide switching frequency range. Currently, for traction applications, Silicon Carbide (SiC) devices are the most used technology. However, as shown in [1], Gallium Nitride (GaN) devices are gaining attention due to their superior switching transitions. This technology presents a current limitation due to its structure. Therefore, its investigation for EVs is not abundant. The implementation of WBG devices presents some challenges such as the Common Mode Voltage (CMV) due to their high dv/dt , Electromagnetic interference (EMIs), insulation failure, and sensor disturbances [2].

The reliability problem is faced with the implementation of multiphase machines ($n > 3$). The characteristic

redundancy of the multiphase machine allows the implementation of a fault-tolerant control. In this way, human safety is ensured, and the drive continues working under open-phase or short-circuit fault. [3]. Besides that, in comparison with their three-phase counterparts, the rating power of the devices is reduced since the current of the inverter is divided into n branches. The rating power reduction when multiphase drives are implemented, enables the implementation of GaN devices, tackling the problem of current limitations.

The implementation of multiphase machines also offers a degree of freedom that can be applied to improve the performance of the drive's control. Applying Clarke's transformation to a multiphase machine, $(n - 1)/2$ two-dimensional subspaces and one-dimensional subspace are achieved for odd n number of phases. On the contrary, for even n number of phases, $n/2$ subspaces are achieved [4]. In Vector Control (VC), only two independently controllable currents are required for the control of the motor. Hence, the remaining subspaces can be used for the control of the low-order harmonics [5]. In [6] PI regulators are implemented for each plane to reduce the harmonics of the plane. However, when asymmetries in the machine are present, an AC component appears. This AC component cannot be controlled by these types of regulators. To face this problem, a dual PI regulator is presented in [7] where the effectiveness of the proposed current regulators is validated experimentally for a Dual Three-phase Induction Machine (IM).

As mentioned in [8], the bandwidth requirement of the current controller is a constraint for the maximum limit of the motor's fundamental frequency. To maintain a good control of the drive, a suitable $[> 21]$ switching to the fundamental frequency ratio m_f is necessary. When the control of low-order harmonics in multiphase machines is considered, the bandwidth requirement for the current controllers of these subspaces is $m_f = f_{sw}/5f_e$. To be able to fulfill this condition, a high switching frequency is required to achieve high fundamental frequencies.

Therefore, the implementation of WBG with multiphase machines is a great combination.

WBG devices allow high switching frequency ranges and low switching and conduction losses. To improve the performance of the drive when this type of semiconductors are used, variable switching frequency controls are implemented. In [9], an optimal switching loss reduction control using variable switching frequency for a three-phase system is presented. The optimization constraint in this control is the output current ripple rms value. Experimental tests were conducted, showing nearly a 19% reduction in the switching losses. To satisfy the ripple requirements, two methods were discussed in [10] to achieve higher efficiency and EMI attenuation. Another objective for the implementation of variable switching frequency control is to improve the overall efficiency of the drive. This type of control was presented in [11] with a three-phase drive based on GaN semiconductors. The proposed control is validated experimentally achieving around a 1.5% improvement and the total loss is reduced by about 10%.

In this paper, the performance of an asymmetric six-phase drive based on GaN inverter under a variable switching control is analysed. In Section 2, the characteristics of the considered multiphase GaN drive are presented. The simulation results obtained with the proposed control for the drive are presented in Section 3. In addition, the switching and conduction loss results are analysed. Finally, in Section 4, the conclusions obtained in this work are presented.

2. Multiphase Drive Characteristics

In this section, the drive is discussed. First, the characteristics of the inverter and the machine are shown. For the control of the drive, the TMS320F28379D microcontroller is used. In Fig.1 the block diagram of the multiphase GaN drive is shown.

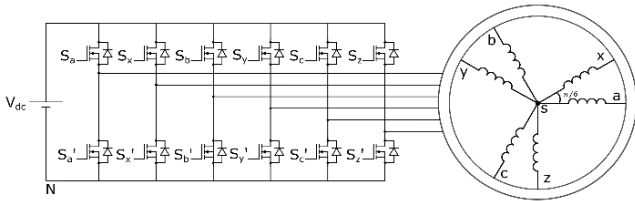


Fig. 1: Block Diagram of the multiphase GaN-based drive.

On the one hand, the inverter is a six-leg two-level GaN-based inverter. This inverter has a DC-link of 400V, a peak current of 20Arms and its maximum frequency is $f_{sw} = 40\text{kHz}$. More information about the inverter can be found in [12].

On the other hand, the machine is an asymmetric six-phase Interior Permanent Magnet Synchronous Machine (A6IPMSM). As can be seen in Fig.1, the two three-phase sets are displaced $\gamma = 30^\circ$. The characteristics of the A6SPWM are shown in Table I.

Table 1: Characteristics of the A6IPMSM.

Parameter	Value	Parameter	Value
n	6	I_{rat}	20Arms
p	4	R_s	0.337 Ω
P_{rat}	19kW	λ_{pm}	117mWb

N_{mec}	3000rpm	L_d	2.5mH
T_{em}	98Nm	L_q	6.1mH

For an asymmetric six-phase machine, the sinusoidal phase voltage waveforms for a two-level inverter topology are defined by (1).

$$v_{ph} = A \cos\left(\omega t - k \frac{\pi}{6}\right) \quad (1)$$

where $k = 0, 1, 4, 5, 8$ and 9 which corresponds to the phase-shift correspondent to the phases a, x, b, y, c, z .

3. Multiphase Drive Control

In this section, the implemented vector control and variable switching frequency are presented. The obtained simulation results are analysed.

A. Vector Control

The implemented control technique is the Indirect Rotor Field Oriented Control (IRFOC). The dq -currents' references are obtained with the Maximum Torque Per Ampere (MTPA) algorithm. Due to the redundancy of multiphase machines, $n - 1$ pair of planes exists, which in a six-phase machine are $\alpha\beta$ -, xy - and 0_+0_- -planes. In $\alpha\beta$ -plane the control of the fundamental is done, while in the other planes, only losses are generated due to the harmonics. In Table 2, the harmonics in each plane are shown.

Table 2: Harmonic mapping for a Dual Three-phase Machine.

Plane	Harmonic
$\alpha\beta$	$1^{st}, 11^{th}, 13^{th}$
xy	$5^{th}, 7^{th}$
0_+0_-	$3^{rd}, 6^{th}, 9^{th}$

In this paper, the degrees of freedom are used to minimize the harmonics of these planes and improve the performance of the drive, since is a critical factor in the EVs. In Fig.2, the implemented control block diagram is shown. To control the low-order harmonics, two PI current regulators are implemented in each subspace. For the conversion from phase variables to dq rotational frame, Clarke (2) and Park transformations are applied [4]. Regarding the modulation, the 6^{th} harmonic injection Pulse Width Modulation (PWM) is implemented. Since this technique injects the zero-sequence harmonic, from now on, it is referred to as Zero Sequence Injection PWM (ZIPWM).

$$\begin{bmatrix} f_\alpha \\ f_\beta \\ f_x \\ f_y \\ f_{0+} \\ f_{0-} \end{bmatrix} = \frac{2}{6} \begin{bmatrix} 1 & \cos \alpha & \cos 4\alpha & \cos 5\alpha & \cos 8\alpha & \cos 9\alpha \\ 0 & \sin \alpha & \sin 4\alpha & \sin 5\alpha & \sin 8\alpha & \sin 9\alpha \\ 1 & \cos 5\alpha & \cos 8\alpha & \cos \alpha & \cos 4\alpha & \cos 9\alpha \\ 0 & \sin 5\alpha & \sin 8\alpha & \sin \alpha & \sin 4\alpha & \sin 9\alpha \\ 1 & 0 & 1 & 0 & 1 & 0 \\ 0 & 1 & 0 & 1 & 0 & 1 \end{bmatrix} \quad (2)$$

B. Variable Switching Control

As mentioned before, to improve the efficiency of the drive, a variable switching frequency is implemented. In this work, the objective of the variable switching frequency control is to maintain the frequency ratio

$m_f=17$. In Fig. 3 the switching frequency in function of the reference speed is shown. As can be seen, as the speed of the machine increases, the switching frequency increases too in order to maintain the m_f ratio constant.

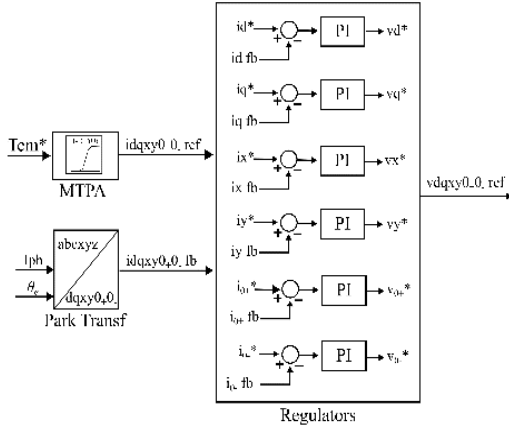


Fig. 2: Block diagram of the control for A6IPMSM and GaN-based drive.

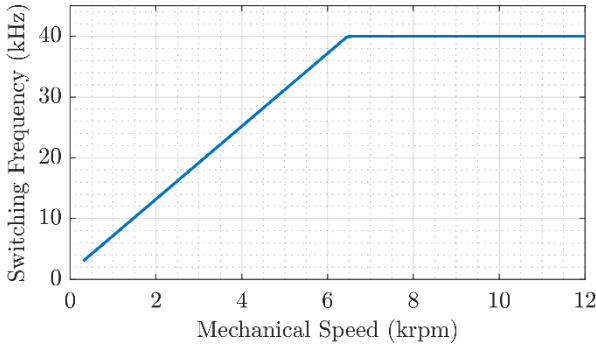


Fig. 3: Switching frequency values depending on the fundamental mechanical speed N_{mec} .

To analyse the performance of the drive when the switching frequency control is applied, simulation results of the torque, current, and voltages are shown. For that, three different speed steps are applied in the constant torque region. These fundamental speed values are $N_{mec} = 1725\text{rpm}$, $N_{mec} = 2250\text{rpm}$ and $N_{mec} = 2700\text{rpm}$. This profile is shown in Fig. 4. The implemented dead time in the semiconductors to avoid the shortcircuit is $t_d = 80\text{ns}$.

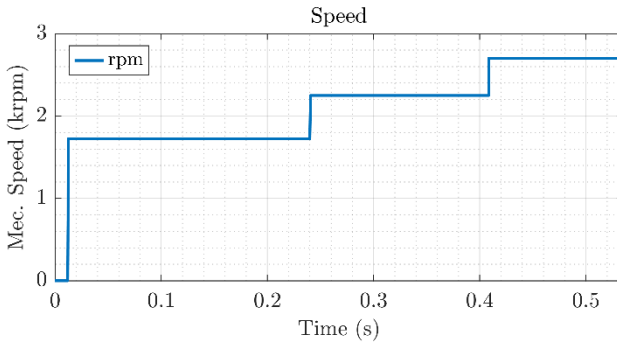


Fig. 4: Applied speed profile for the implemented variable switching frequency control.

The selected switching frequency for each speed step is shown in Fig. 5. As mentioned before, the switching frequency is selected to maintain a frequency ratio $m_f =$

17. A minimum value of 1kHz is set to maintain a good control when the speed of the machine is zero.

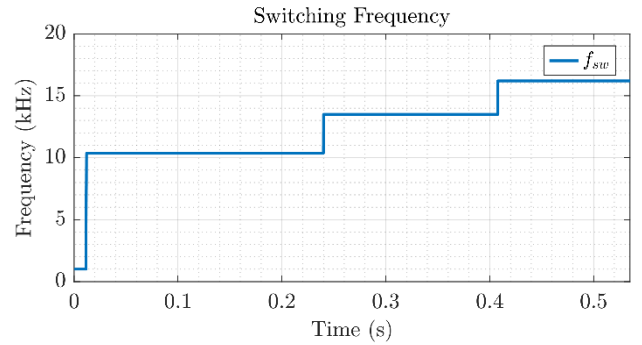


Fig. 5: Selected switching frequency for the implemented variable switching frequency control.

When the switching frequency of the inverter is changed depending on the fundamental speed of the machine, the sampling time of the control is varied as $T_s = 1/f_{sw}$. In the following paragraphs, the results obtained when the sample time is changed are analysed. First, torque, phase current and voltage amplitude of the phase voltage are studied. After that, voltage and current in the rotational frame are analysed. Finally, torque ripple (ΔT_{em}) and current Total Harmonic Distortion (THD) for the three analysed working points are shown. Besides that, the analysis of the current in the frequency domain is done to study the impact of the variable switching frequency control.

In Fig. 6 the reference and measured torque are shown. A torque step from 0 to T_{rat} is applied. It can be seen that the first part has the highest torque ripple in comparison with the other two analysed working points. This region is the one that has the higher sampling rate the lower fundamental speed. However, as the speed is increased, the torque ripple is improved.

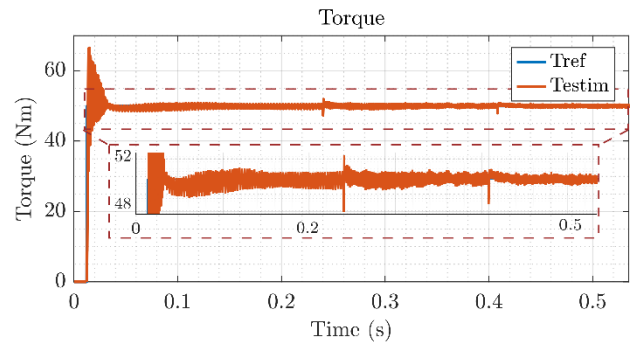


Fig. 6: Simulation results of the torque reference (blue) and torque of the AS6IPMSM (red) for the implemented variable switching frequency control.

The three analysed working points are in the constant torque region. Thus, the amplitude of the current in these points must be equal to the current rated value. In Fig. 7, it can be seen that the implemented variable switching frequency control fulfils this requirement.

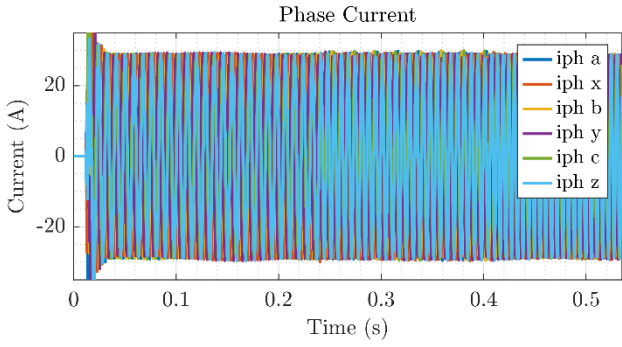


Fig. 7: Simulation results of phase current for the implemented variable switching frequency control.

To see with more clarity the effect of the transitions between the analysed working points, Fig. 8 is presented. In the top part of this figure, the transition from $N_{mec}=1725rpm$ to $N_{mec}=2250rpm$ at $t=240ms$ is shown. It can be seen that the frequency of the current is increased as expected while maintaining a sinusoidal waveform. At the bottom part of Fig. 8, the transition from $N_{mec}=2250rpm$ to $N_{mec}=2700rpm$ at $t=408ms$ can be seen. In this case, a sinusoidal current waveform is also maintained after the transition.

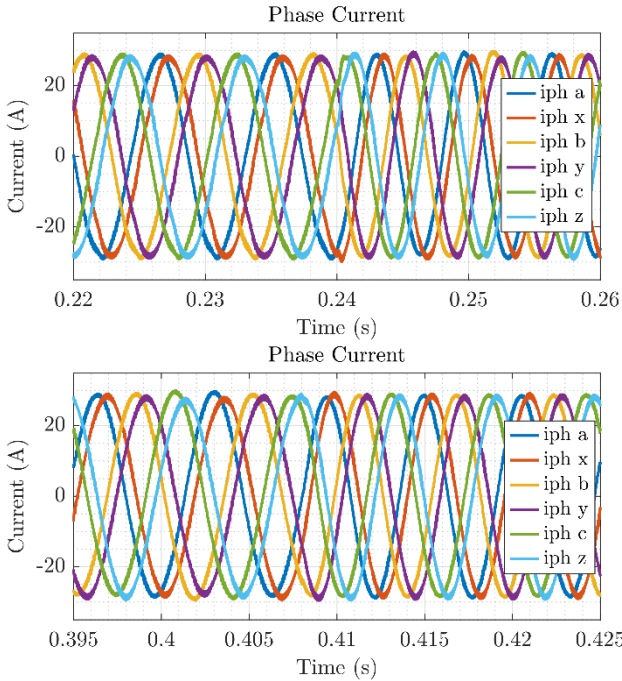


Fig. 8: Phase current transition from $N_{mec}=1725rpm$ to $N_{mec}=2250rpm$ at $t=240ms$ (top) and from $N_{mec}=2250rpm$ to $N_{mec}=2700rpm$ at $t=408ms$ (bottom).

The estimated phase voltage amplitude is shown in Fig. 9. It can be seen that the amplitude of the phase voltage is higher as the fundamental speed is increased, as expected. It can be noted that the third analysed working point is very close to the rated phase voltage of the machine. This fact points out that this speed is very near to the speed base value of the machine.

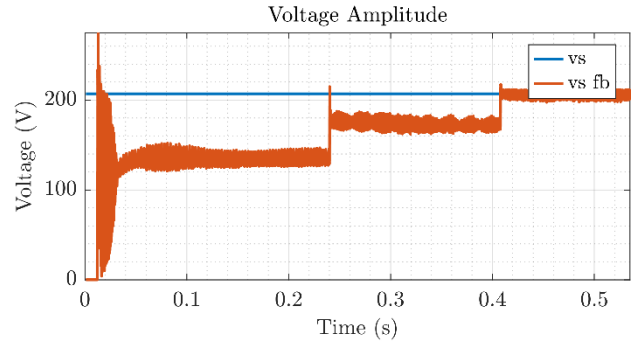


Fig. 9: Maximum voltage amplitude of the machine (blue) and estimated voltage amplitude of the machine (red).

As shown in the control block diagram, the input references to the current controller regulators are the d-axis current i_d and the q-axis current i_q . These references and their respective feedback signals are shown in Fig. 10. As in the torque variable, it can be seen how the current ripple is reduced as the fundamental speed increases. The tracking of the control of both currents is done correctly in the three analysed working points when the variable switching frequency control is applied.

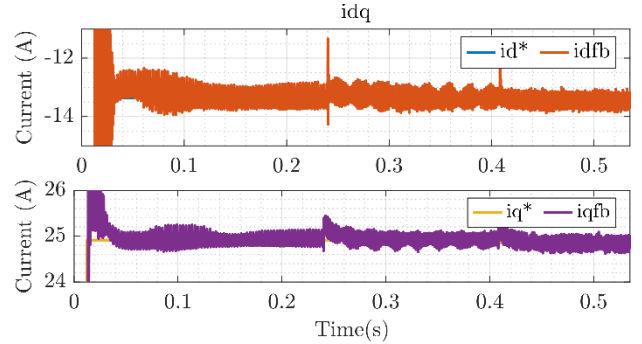


Fig. 10: Current in dq axis (i_{dq}) for the three analysed working points.

As explained before, the degree of freedom of the multiphase machine in this work is used for the control of the harmonics placed in the subplanes to be equal to zero. The resultant feedback current for the xy -subplane is shown in Fig. 11. It can be noted that the maximum amplitude of the current in the xy -subplane is 6.51% of the rated current value, which can be considered a good reduction of the 5th harmonic. The error between the referenced and the measured signals is higher as the fundamental speed is increased. The reason for that is that the bandwidth limit of the current controller in this plane is being reached. However, a good control is maintained.

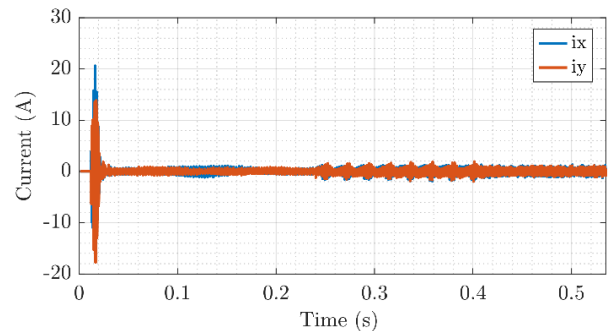


Fig. 11: Currents in xy -plane for the implemented variable switching frequency control.

The output of the current controller regulators is the voltages v_{dq} and v_{xy} . In Fig. 12, the fundamental voltage values reference v_{dq} are shown. It can be seen how the v_d voltage amplitude is higher as the fundamental speed is increased whereas the voltage v_q is lower. The reason for that is that as the fundamental speed increases, the phase voltage amplitude must be maintained within the limits of the rated voltage value. Therefore, the voltage in the d-axis is increased to deflux the machine.

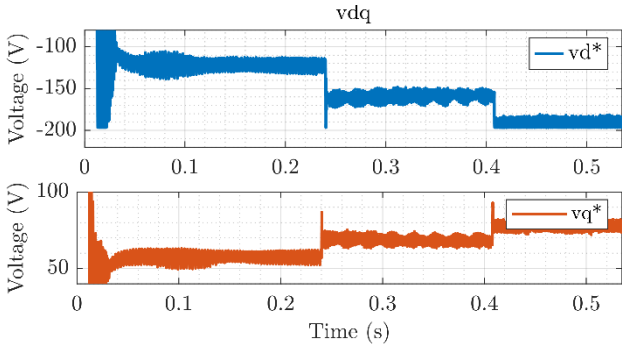


Fig. 12: Voltages in dq -axis (v_{dq}) for the three analysed working points.

The resultant voltages references in the xy -subplane are shown in Fig. 13. The amplitudes of these reference voltages are almost zero. The percentages of the v_{xy} respect to the phase voltage amplitudes are 0.074%, 0.314% and 0.628 for $N_{mec}=1725$ rpm, $N_{mec}=2250$ rpm and $N_{mec}=2700$ rpm, respectively. Thus, it can be concluded that the control aimed to the reduction of the low-order harmonics works as expected.

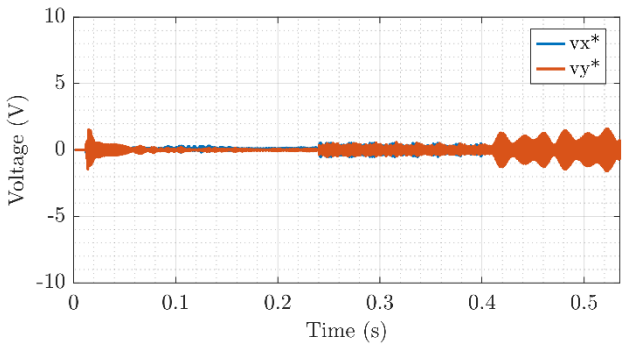


Fig. 13: Voltages in the xy -axis (v_{xy}) for the three analysed working points.

In Table 3 the switching frequency, torque ripple and current THD for each analysed speed working points are analysed. The resultant torque ripple for $N_{mec} = 1725$ rpm and $N_{mec} = 2250$ rpm, are of similar values. On the contrary, for $N_{mec} = 2700$ rpm the torque ripple is reduced a 66.7% respect to the previous fundamental speed. For the lowest fundamental speed, which results in the lowest switching frequency and sample time of the control, the worst results are obtained regarding the THDi. However, the second and third analysed speed points achieve similar THDi values which are 2.80% and 2.17%, respectively. As mentioned before, the switching frequency of the inverter is higher as the fundamental speed increases. Thus, it can be concluded that a good control is achieved when the variable switching frequency control is implemented.

Table 3: Switching frequency, current THD and torque ripple values for the analysed working points.

N_{mec}	f_{sw}	ΔT_{em}	THD_i
1725 rpm	10.35kHz	2.78%	7.18%
2250 rpm	13.5kHz	2%	2.80%
2700 rpm	16.2kHz	1.20%	2.17%

C. Power Losses

The variable switching frequency aims to reduce the switching losses of the semiconductor. In this section, a comparison of the conduction and switching losses is done between the variable switching frequency control and a constant switching frequency. In this case, the constant switching frequency value is $f_{sw} = 20$ kHz since GaN devices are used. The studied working points are the ones analysed in the previous section: $N_{mec}=1725$ rpm, $N_{mec}=2250$ rpm and $N_{mec}=2700$ rpm.

In Fig. 14 a comparison of the conduction losses between the variable switching frequency control and fixing a constant switching frequency of 20kHz in the three analysed speed point is shown. The conduction losses are slightly lower when the switching frequency is fixed to 20kHz, since it results in a faster sample time of the control.

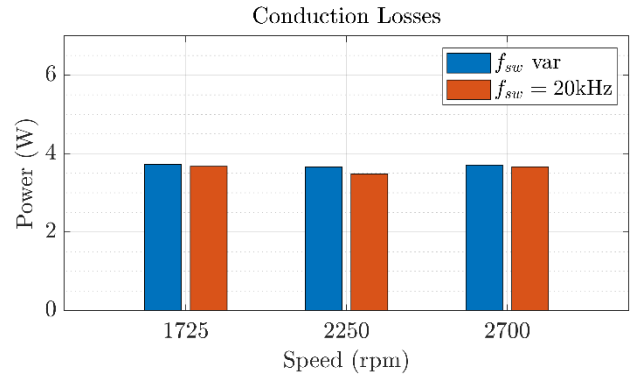


Fig. 14: Conduction Losses for the three analysed speed values.

The resultant switching losses obtained for both scenarios in the three analysed speed points are shown in Fig. 15. When the variable switching frequency is implemented, lower switching losses are obtained in comparison with the constant switching frequency of 20kHz. For the first analysed speed point, a reduction of 40.51% is obtained when the variable switching frequency control is selected. At $N_{mec} = 2250$ rpm, the switching losses are reduced by 38.62% and at $N_{mec} = 2700$ rpm by 30.43%.

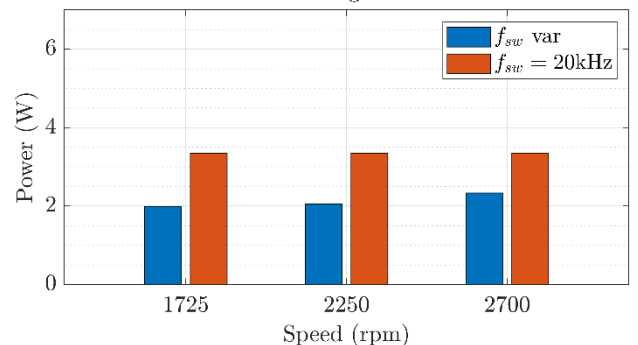


Fig. 15: Switching Losses for the three analysed speed values.

Hence, the implementation of the variable switching frequency improves the efficiency of the EV's drive since the switching losses are reduced. This benefit tackles one of the EVs problems which extend the autonomy of the EV.

4. Conclusions

In this paper, the performance of the variable switching frequency control for an asymmetric six-phase motor and a GaN-based inverter is analysed. One of the characteristics of the GaN devices is that they allow a high range of switching frequency and the reduction of power losses in comparison with other technologies, such as Silicon.

The simulations are done in three different fundamental speed points: $N_{mec} = 1725\text{rpm}$, $N_{mec} = 2250\text{rpm}$ and $N_{mec} = 2700\text{rpm}$. Simulation results for measured torque, current and voltages are shown when the variable switching frequency is implemented. The obtained results show a good control performance. Besides that, the conduction and switching losses results are shown. This comparison is done for two different scenarios which are the implementation of the variable switching frequency and a constant switching frequency for the three analysed speed points. This comparison concludes that a reduction higher than 30% is obtained with the variable switching frequency.

To sum up, the variable switching frequency obtains a high reduction in the switching losses which leads to higher efficiencies increasing EV's autonomy.

References

- [1] Turzyński, M.; Musznicki, P. A Review of Reduction Methods of Impact of Common-Mode Voltage on Electric Drives. *Energies* 2021, 14, 4003.
- [2] Power Electronics News, "Wide-Bandgap Semiconductors for EVs – Panel." [Online].
- [3] H. S. Che, M. J. Duran, E. Levi, M. Jones, W.-P. Hew, and N. A. Rahim, "Postfault Operation of an Asymmetrical Six-Phase Induction Machine With Single and Two Isolated Neutral Points," *IEEE Trans. Power Electron.*, vol. 29, no. 10, pp. 5406–5416, Oct. 2014, doi: 10.1109/TPEL.2013.2293195.
- [4] E. Levi. 28 Feb 2011, Multiphase AC Machines from: The Industrial Electronics Handbook, Power Electronics and Motor Drives CRC Press Accessed on: 29 Jun 2021 <https://www.routledgehandbooks.com/doi/10.1201/b10643-6>.
- [5] E. Levi, F. Barrero and M. J. Duran, "Multiphase machines and drives - Revisited," in *IEEE Transactions on Industrial Electronics*, vol. 63, no. 1, pp. 429-432, Jan. 2016, doi: 10.1109/TIE.2015.2493510. keywords: {Special issues and sections;Inverters;Fault tolerance;Motor drives;Circuit faults;Induction machines;Harmonic analysis;Pulse width modulation;Windings}.
- [6] Tounsi Kamel, Djehbar Abdelkader, and Barkat Said. "Vector control of five-phase permanent magnet synchronous motor drive". In: 2015 4th International Conference on Electrical Engineering (ICEE). 2015, pp. 1–4. doi: 10.1109/INTEE.2015.7416853.
- [7] Hang Seng Che et al. "Current Control Methods for an Asymmetrical Six-Phase Induction Motor Drive". In: *IEEE Transactions on Power Electronics* 29.1 (2014), pp. 407–417. doi: 10.1109/TPEL.2013.2248170.
- [8] I. Husain et al., "Electric Drive Technology Trends, Challenges, and Opportunities for Future Electric Vehicles," *Proc. IEEE*, vol. 109, no. 6, pp. 1039–1059, 2021.
- [9] Oier Oñederra et al. "Three-Phase VSI Optimal Switching Loss Reduction Using Variable Switching Frequency". In: *IEEE Transactions on Power Electronics* 32.8 (2017), pp. 6570–6576. doi: 10.1109/TPEL.2016.2616583.
- [10] Dong Jiang and Fei Wang. "Variable Switching Frequency PWM for Three-Phase Converters Based on Current Ripple Prediction". In: *IEEE Transactions on Power Electronics* 28.11 (2013), pp. 4951–4961. doi: 10.1109/TPEL.2013.2240701.
- [11] Kazuki Ohta et al. "Variable Switching Frequency Control for Efficiency Improvement of Motor Drive System by Using GaN Three Phase Inverter". In: 2020 IEEE International Conference on Industrial Technology (ICIT). 2020, pp. 119–123. doi: 10.1109/ICIT45562.2020.9067266.
- [12] Carrasco, M., Gondat, M., Avila, A., Lopez de Heredia, A & Almandoz, G. GaN Based Multiphase Drive for Electric Vehicles in PCIM Europe 2023; 1–5.